NUMERICAL STUDY OF HYDROGEN IGNITION BY PASSIVE AUTO-CATALYTIC RECOMBINERS

N. Meynet[a*], A. Bentaib[a]

[a] *Institut de Radioprotection et de Sûreté Nucléaire (IRSN), Direction de la sûreté des réacteurs, Service d'évaluation des accidents graves et des rejets radioactifs - BP 17, 92262 Fontenay aux Roses, France*
[*] *Corresponding author: nicolas.meynet@irsn.fr*

Passive Auto-catalytic Recombiners (PARs) are used to avoid excessive hydrogen accumulation inside reactor containment in case of severe accident. Most of them are constructed using catalytic materials (bed of beads or row of vertical plates with platinum and palladium on ceramic washcoat) and housed in a metallic structure. Their behavior is based on the exothermic recombination of hydrogen into steam in presence of oxygen. This surface mechanism leads to an overheating of the catalytic plates and activates natural convection driven circulation of gases in contact with the catalyst. Now, the heat source induced by the PAR activity can create local conditions for hydrogen gaseous combustion, as igniters do.

This paper deals with PAR hydrogen ignition limit according to a variety of thermal-hydraulics conditions. The catalytic hydrogen ignition is characterized by a detailed analysis of the flow structure and of the chemical mechanisms. A physical criterion is proposed for identifying PAR hydrogen ignition, and is applied for a wide range of inlet conditions. The resulting PAR hydrogen ignition map is then validated on the basis of an experimental database.

I. INTRODUCTION

In the hypothetical case of a severe accident in a nuclear reactor with core meltdown, the interaction of the hot core with the cooling water can generate large amounts of hydrogen. It can also result from the oxidation of metals present in the corium pool or in the basemat during the molten corium-concrete interaction phase. This hydrogen is transferred into the containment (and transported therein) by convection loops arising essentially from condensation of steam released via the break in the reactor cooling system or during corium-concrete interaction. Depending on mixing in the containment atmosphere, the distribution of hydrogen is more or less homogeneous. If considerable hydrogen stratification exists, then local concentration of hydrogen may become substantial, and may exceed the lower flammability limit. In case of ignition, the subsequent pressure loads may adversely affect the containment.

To limit the hydrogen concentration in the containment, several methods can be proposed. For pressurized water reactors (PWRs), the hydrogen mitigation strategy usually consists in combining large free volume to allow atmosphere dilution, a high value of the containment design pressure and the use of means, as passive autocatalytic recombiners to consume hydrogen. This strategy has been adopted in all French PWRs.

To support this decision, specific experimental set-ups have been conducted by manufacturers as AREVA, research institutes as CEA, or technical safety organizations as IRSN, with the aim to characterize PARs efficiency in representative severe accident conditions. The performed experimental tests showed that for specific conditions, PARs could induce combustion. Based on this experimental data, it seems that ignition induced by recombiners occurs for low hydrogen concentrations, leading to relatively low overpressure. Hence, PARs ignition could have a beneficial effect (Ref. 1). Nonetheless, these experiments results need to be corroborated by more detailed experiments and by refined modeling of phenomena occurring in PARs.

This paper aims to present a new approach for PAR modeling based on complex chemical kinetics and detailed multi-component transport. This model is used to characterize the hydrogen ignition inside PARs and to determine the PAR hydrogen ignition limit. The numerical results are then compared to the available experimental database.

II. EXPERIMENTAL DATA

Several experiments have been performed in the past to investigate the PARs behavior in representative severe accident conditions, among them the H2PAR experimental program (Ref. 2) conducted by IRSN

(formerly IPSN). One of the main topics addressed in this program was the characterization of PARs ignition conditions. Numerous tests have been realized at atmospheric pressure with different initial gas composition. Under specific conditions, flame could be observed in the lower edge of the PAR (Fig. 1).

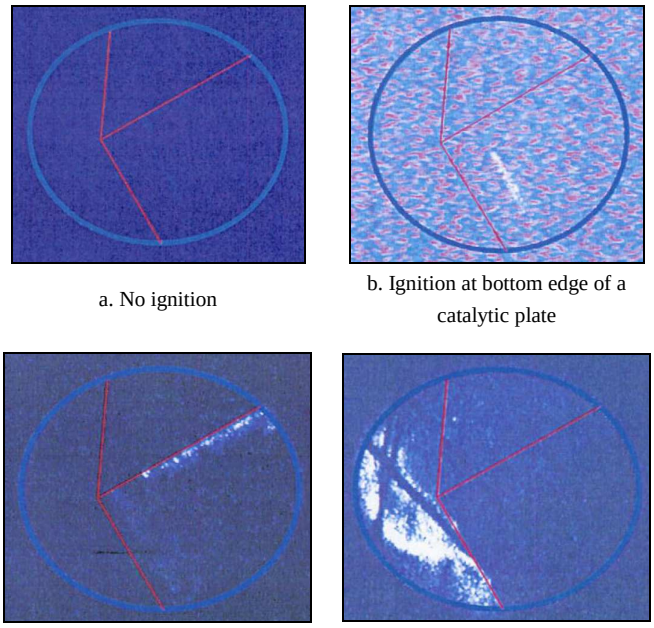

a. No ignition

b. Ignition at bottom edge of a catalytic plate

c. Combustion propagation to the bottom edge of the PAR box

d. Combustion propagation outside the PAR box

Fig. 1. Experimental visualization with a UV camera of the hydrogen ignition and combustion propagation inside PARs (the red lines represent the contour of the PAR box and the blue circle the camera scope)

The main results of these PAR ignition tests show that ignition induced by recombiners occurs for low hydrogen concentrations respecting to the following limits (Ref. 3):

- in dry air, a generalized ignition was observed for hydrogen molar fraction between 5.5% and 6.8%,
- at 9.2% steam initial molar fraction, a generalized ignition was detected for an hydrogen molar fraction of 8.5%,
- at 31% steam initial molar fraction, ignition appeared for an hydrogen molar fraction around 8.6%,
- at 45% steam initial molar fraction, ignition occurred for an hydrogen molar fraction around 10%.

These results are in good agreement with experiments from the KALI-H2 program (Ref. 4) conducted by CEA. They were recently corroborated by PAR ignition tests performed in the frame of the OECD THAI project (Ref. 5).

III. SPARK CODE

In this section, we describe a numerical tool developed by IRSN dedicated to catalytic reactor-type applications. Its name SPARK is the acronym of Simulation for Passive Autocatalytic Recombiners' risK. This code solves the two-dimensional steady-state Navier-Stokes equations in the vorticity-velocity formulation by including complex gas phase and surface chemistry, multi-component transport, and heat radiation (Refs. 6-7).

III.A. Numerical domain

The numerical domain is derived from the box-type PARs with row of vertical catalytic sheets as illustrated in Fig. 2. We suppose infinitely thin catalytic plates, so that solid heat conduction is neglected. Moreover, external heat losses are not taken into account. As a result, the flow is supposed to be symmetrical and the numerical domain is reduced to a half-channel between two catalytic plates in the median plane (Fig. 2).

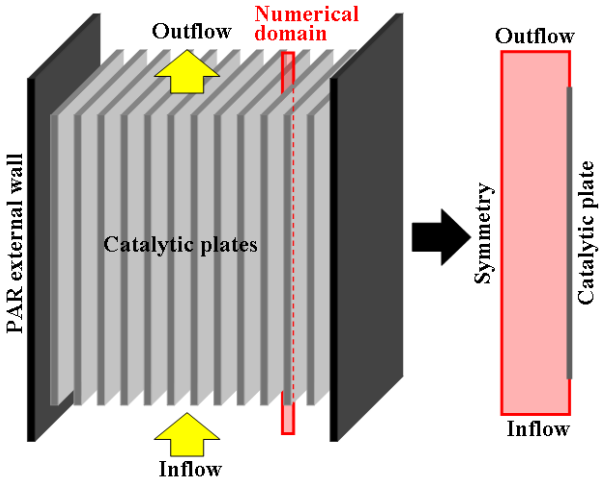

Fig. 2. Schematic of catalytic sheets inside PARs (left) and numerical domain (right)

III.B. Governing equations

The governing equations express the conservation of total mass, momentum, energy, and species mass, for two-dimensional planar reactive flows. We use a modified vorticity-velocity formulation of the Navier-Stokes equations (Ref. 8) which is more effective at conserving mass than the standard one (Ref. 9).

The gas phase equations may be written as follows:

- Horizontal velocity

$$\partial^2_{xx}u+\partial^2_{yy}u=\partial_y\omega-\partial_x\left(\frac{u}{\rho}\partial_x\rho+\frac{v}{\rho}\partial_y\rho\right), \qquad (1)$$

- Vertical velocity

$$\partial^2_{yy} v = -\partial^2_{xy} u - \partial_y \left(\frac{u}{\rho} \partial_x \rho + \frac{v}{\rho} \partial_y \rho \right), \quad (2)$$

- Vorticity

$$\begin{aligned} &\partial^2_{xx}(\mu\omega) + \partial^2_{yy}(\mu\omega) = \rho u \partial_x \omega + \rho v \partial_y \omega \\ &+ \partial_y \rho \partial_x (u^2/2) - \partial_x \rho \partial_y (v^2/2) + \partial_x \rho g \\ &+ 2\partial_x \mu \, \partial_y (\partial_x u + \partial_y v) - 2\partial_y \mu \, \partial_x (\partial_x u + \partial_y v) \\ &+ 2\partial_y u \partial^2_{xx} \mu - 2\partial_x v \partial^2_{yy} \mu - 2\partial_x u \partial^2_{yx} \mu + 2\partial_y v \partial^2_{xy} \mu, \end{aligned} \quad (3)$$

- Gaseous species mass

$$\begin{aligned} \rho u \partial_x Y_k + \rho v \partial_y Y_k = &-\partial_x (\rho Y_k U_k) - \partial_y (\rho Y_k V_k) \\ &+ M_k \omega_k \quad \text{for} \quad k = 1 \ldots n, \end{aligned} \quad (4)$$

- Energy

$$\begin{aligned} &\rho c_p u \partial_x T + \rho c_p v \partial_y T = \partial_x (\lambda \partial_x T) + \partial_y (\lambda \partial_y T) \\ &- \sum_{k=1}^{n} \rho c_{pk} Y_k (U_k \partial_x T + V_k \partial_y T) - \sum_{k=1}^{n} h_k M_k \omega_k, \end{aligned} \quad (5)$$

where ρ is the density, u the horizontal velocity, v the vertical velocity, T the temperature, Y_k the mass fraction of the k^{th} species, ∂_x the space derivative operator, g the gravitational acceleration, μ the shear viscosity of the mixture, U_k and V_k the horizontal and vertical diffusion velocity of the k^{th} species, M_k the molar mass of the k^{th} species, ω_k the gas phase molar production rate of the k^{th} species, c_p the specific constant pressure heat capacity of the mixture, λ the thermal conductivity of the mixture, n the number of gaseous species, h_k the specific enthalpy of the k^{th} species and c_{pk} its specific constant pressure heat capacity. The vorticity ω is classically defined by:

$$\omega = \partial_y u - \partial_x v. \quad (6)$$

One additional equation expresses the absence of surface species inside the gas flow:

$$\sigma_k = 0 \quad \text{for} \quad k = 1 \ldots \hat{n}, \quad (7)$$

where σ_k is the site fraction occupancy of the k^{th} species, and $\hat{n}$ the number of surface species. Finally, to complete the governing equations, the low Mach number approximation allows to write the ideal gas law as follows:

$$\rho = \frac{p_0 \overline{M}}{RT}, \quad (8)$$

where $\overline{M}$ is the mean molar mass of the mixture, R the universal gas constant, and p_0 the ambient pressure.

III.C. Boundary conditions

III.C.1. Catalytic surface

The boundary condition on the catalytic surface expresses the conservation of species mass and energy through a solid-gas reactive interface, and the no-slip conditions. These balance equations may be written as follows:

- Horizontal and vertical velocities

$$u = v = 0, \quad (9)$$

- Gaseous species mass

$$\rho Y_k U_k = -M_k \hat{\omega}_k \quad \text{for} \quad k = 1 \ldots n, \quad (10)$$

- Surface species mass

$$\hat{\omega}_k = 0 \quad \text{for} \quad k = n+1 \ldots n+\hat{n} \quad (11)$$

- Energy

$$\lambda \partial_x T = -\sum_{k=1}^{n+\hat{n}} h_k M_k \hat{\omega}_k - q^{rad} \quad (12)$$

where $\hat{\omega}_k$ is the surface molar production rate of the k^{th} species and q^{rad} the radiative heat flux. The equation (11) expresses that we consider no mass accumulation on the catalytic surface.

III.C.2. Inlet

The boundary condition on the inlet expresses the estimated experimental conditions at PARs inlet. We consider uniform profiles for all the variables:

$$\begin{aligned} &u = 0, \quad v = v_{in}, \quad \omega = \partial_y u - \partial_x v, \quad T = T_{in}, \\ &\rho Y_k^{in} v_{in} = \rho Y_k (v + V_k) \quad \text{for} \quad k = 1 \ldots n, \end{aligned} \quad (13)$$

where v_{in} is the inlet vertical velocity, Y_k^{in} the inlet mass fraction of the k^{th} species, and T_{in} the inlet temperature.

III.C.3. Outlet

The boundary condition on the outlet sets the vertical derivatives to zero:

$$\begin{aligned} &u = 0, \quad \partial_y v = 0, \quad \partial_y \omega = 0, \\ &\partial_y T = 0, \quad \partial_y Y_k = 0 \quad \text{for} \quad k = 1 \ldots n. \end{aligned} \quad (14)$$

III.C.4. Symmetry

The boundary condition on the symmetry axis sets the horizontal derivatives to zero:

$$u = 0, \quad \partial_x v = 0, \quad \omega = 0,$$
$$\partial_x T = 0, \quad \partial_x Y_k = 0 \quad \text{for} \quad k = 1 \ldots n. \tag{15}$$

III.D. Transport

The different transport coefficients which appear in the governing equations (shear viscosity, conductivity, diffusion coefficients) are derived from the kinetic theory of gases (Ref. 10). They are evaluated using multi-component transport algorithms (Ref. 11). The species diffusion velocities are then given by:

$$U_k = -\sum_{l=1}^{n} D_{kl} \partial_x X_l - \theta_k \partial_x (\log T) \quad \text{for} \quad k = 1 \ldots n, \tag{16}$$

where X_l is the molar fraction of the l^{th} species, D_{kl} the species diffusion coefficients and θ_k the thermal diffusion coefficient of the k^{th} species. This definition includes the multi-component diffusion (i.e. each species diffuses in relation to all the other species) and the thermal species diffusion (or Soret effect). Moreover, this formulation intrinsically satisfies the total mass conservation constraint:

$$\sum_{k=1}^{n} Y_k V_k = 0, \tag{17}$$

which often limits the use of Fick-type expressions in multi-component reactive flows.

III.E. Chemical kinetics

The molar gas phase and surface production rates are derived from detailed chemical mechanisms. The molar production rate of each species in the gas or on the surface results from the sum of its molar production rates over the reactions described in the next tables. The gas phase chemical kinetics which includes 9 gaseous species for 19 reactions (Tab. 1), was proposed by Warnatz et al (Ref. 12). The surface chemical kinetics (Tab. 2) is due to Deutschmann et al (Ref. 13). It includes 5 surface species and 6 gaseous species for 13 reactions. The surface site density is estimated from the density of Platinum (Ref. 14) and is taken as $S_0 = 2.06\ 10^{-9}$ mol/cm^2. Both chemical mechanisms have been successfully validated for applications in a catalytic channel combustor (Ref. 15). Their combination allows a relevant estimation of the ignition distance inside a catalytic reactor for hydrogen/air mixtures.

Tab. 1 Gas phase chemical mechanism

Reactions	A (c.g.s)	n	E (cal/mol)
1. $H + O_2 \Leftrightarrow O + OH$	$2.00\,10^{14}$	0.00	16802.10
2. $O + H_2 \Leftrightarrow H + OH$	$2.06\,10^{04}$	2.67	6285.85
3. $H_2 + OH \Leftrightarrow H_2O + H$	$1.00\,10^{08}$	1.60	3298.28
4. $2\,OH \Leftrightarrow O + H_2O$	$1.50\,10^{09}$	1.14	100.38
5. $H + H + M \Leftrightarrow H_2 + M$	$1.80\,10^{18}$	−1.00	0.00
6. $2\,O + M \Leftrightarrow O_2 + M$	$2.90\,10^{17}$	−1.00	0.00
7. $H + OH + M \Leftrightarrow H_2O + M$	$2.20\,10^{22}$	−2.00	0.00
8. $H + O_2 + M \Leftrightarrow HO_2 + M$	$2.30\,10^{18}$	−0.80	0.00
9. $HO_2 + H \Leftrightarrow H_2 + O_2$	$2.50\,10^{13}$	0.00	693.12
10. $HO_2 + H \Leftrightarrow 2\,OH$	$1.50\,10^{14}$	0.00	1003.82
11. $HO_2 + H \Leftrightarrow H_2O + O$	$3.00\,10^{13}$	0.00	1720.84
12. $HO_2 + O \Leftrightarrow OH + O_2$	$1.80\,10^{13}$	0.00	−406.31
13. $HO_2 + OH \Leftrightarrow H_2O + O_2$	$6.00\,10^{13}$	0.00	0.00
14. $2\,HO_2 \Leftrightarrow H_2O_2 + O_2$	$2.50\,10^{11}$	0.00	−1242.83
15. $2\,OH + M \Leftrightarrow H_2O_2 + M$	$3.25\,10^{22}$	−2.00	0.00
16. $H_2O_2 + H \Leftrightarrow H_2O + OH$	$1.00\,10^{13}$	0.00	3585.09
17. $H_2O_2 + H \Leftrightarrow H_2 + HO_2$	$1.70\,10^{12}$	0.00	3752.39
18. $H_2O_2 + O \Leftrightarrow OH + HO_2$	$2.80\,10^{13}$	0.00	6405.35
19. $H_2O_2 + OH \Leftrightarrow H_2O + HO_2$	$5.40\,10^{12}$	0.00	1003.82

Note. Arrhenius rate coefficients : $k = AT^n exp(-E/RT)$

Tab. 2 Surface chemical mechanism

Adsorption Reactions	s	E
1. $H_2 + 2\,Pt^{(s)} \rightarrow 2\,H^{(s)}$	0.046	–
2. $H + Pt^{(s)} \rightarrow H^{(s)}$	1.000	–
3. $O_2 + 2\,Pt^{(s)} \rightarrow 2\,O^{(s)}$	0.070	–
4. $O + Pt^{(s)} \rightarrow O^{(s)}$	1.000	–
5. $H_2O + Pt^{(s)} \rightarrow H_2O^{(s)}$	0.750	–
6. $OH + Pt^{(s)} \rightarrow OH^{(s)}$	1.000	–
Recombination Reactions	**A**	**E (cal/mol)**
7. $H^{(s)} + O^{(s)} \Leftrightarrow OH^{(s)} + Pt^{(s)}$	$3.70\,10^{21}$	2749
8. $H^{(s)} + OH^{(s)} \Leftrightarrow H_2O^{(s)} + Pt^{(s)}$	$3.70\,10^{21}$	4183
9. $2\,OH^{(s)} \Leftrightarrow H_2O^{(s)} + O^{(s)}$	$3.70\,10^{21}$	11520
Desorption Reactions	**A**	**E (cal/mol)**
10. $2\,H^{(s)} \rightarrow H_2 + 2\,Pt^{(s)}$	$3.70\,10^{21}$	$16109 - 1434\,\sigma_H$
11. $2\,O^{(s)} \rightarrow O_2 + 2\,Pt^{(s)}$	$3.70\,10^{21}$	$50956 - 14340\,\sigma_O$
12. $H_2O^{(s)} \rightarrow H_2O + Pt^{(s)}$	$1.00\,10^{13}$	9632
13. $OH^{(s)} \rightarrow OH + Pt^{(s)}$	$1.00\,10^{13}$	46080

Note. Arrhenius rate coefficients : $k = A exp(-E/RT)$

s sticking coeffcient, σ_k *site occupancy*

III.F. Numerical method

The solution algorithm has been developed on the basis of a laminar Bunsen flame code (Refs. 10,16). The governing equations and boundary conditions are discretized on a two-dimensional tensor-product grid using a finite difference technique (Ref. 17). The resulting system of highly nonlinear coupled equations is solved with a damped Newton's method (Ref. 18). A

preconditioned Bi-CGSTAB algorithm is used to solve the large sparse linear systems arising during Newton iterations (Ref. 19).

Additionally, the numerical evaluation of the chemical production rates, thermodynamical properties, and transport coefficients imposes a particular attention in order to limit the computational cost of the solution. Thus, all properties are calculated using vectorized and highly optimized gas phase chemistry, surface chemistry and transport libraries, respectively named: CHEMKIN II (Refs. 20,21), SURF CHEM (Refs. 6,22), and EGLIB (Ref. 23).

IV. CHARACTERIZATION OF PAR HYDROGEN IGNITION

This section deals with the characterization of PAR hydrogen ignition. It aims at emphasizing the different PAR operation regimes and defining an ignition criterion.

IV.A. Numerical conditions

The numerical domain is a symmetrical planar channel whose width and height are respectively 0.5 cm and 25 cm. The catalytic plate is located at 3 cm from the inlet and is 14.3 cm long. The calculations have been performed by using a regular cartesian mesh with 76 x 151 nodes, and the inlet conditions summarized in Tab. 3. Radiative heat losses and species thermal diffusion are not taken into account.

Tab. 3 Numerical inlet conditions

p_o = 1 atm	0% < X_{H2} < 20%
T_{in} = 298 K	100% > X_{Air} > 80%
v_{in} = 80 cm/s	X_{H2O} = 0%

The inlet velocity is a typical average velocity observed at PAR inlet in experimental devices. As room pressure and temperature were varying during the reference experiments used for this study, these features are chosen at normal conditions. The inlet hydrogen concentration describes a segment between 0 vol.% and 20 vol.% in order to capture the –upper– hydrogen limit without steam.

IV.B. PAR operation regimes

IV.B.1.Qualitative analysis

Before evaluating the PAR hydrogen ignition limit, we study the possible PAR operation regimes in conditions characteristic of hydrogen/air mixtures without steam (i.e. the segment without steam in the ternary diagram H_2–Air–H_2O).

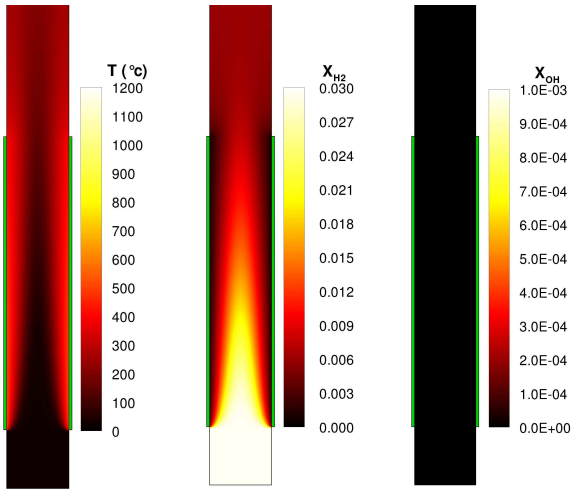

a. $X^{in}_{H_2} = 3\%$

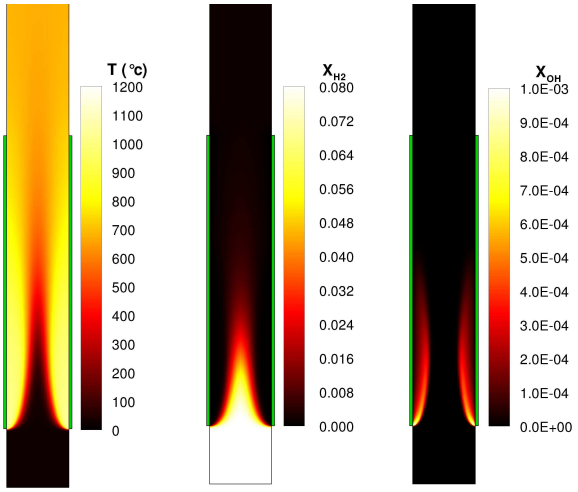

b. $X^{in}_{H_2} = 8\%$

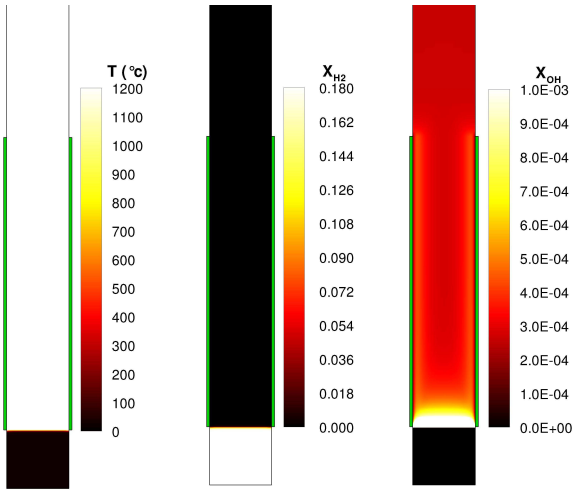

c. $X^{in}_{H_2} = 18\%$

Fig. 3. Flow structures according to PAR operation regime

A first qualitative analysis reveals three types of flow structures and allows a first characterization of PAR hydrogen ignition (Fig. 3). The hydrogen combustion is classically identified with the OH radical. Actually, this species often serves at localizing experimentally the hydrogen or hydrocarbon flame fronts, especially for catalytic reactor applications (Ref. 24).

The highest inlet hydrogen concentration leads to a perfect planar flame structure similar to the one observed in an inert planar channel. In this case, the catalytic activity seems to be negligible. At the opposite, the lowest inlet hydrogen concentration at 3 vol.% does not show any combustion, so that the catalytic processes are predominant. Finally, the flow structure with 8 vol.% of hydrogen at inlet reveals the occurrence of combustion, but with a longitudinal flame front. This intermediate case is more characteristic of catalytically stabilized combustors. Both catalytic and gas phase processes are then important.

IV.B.2.Quantitative analysis

In order to identify more clearly the previous PAR operation regimes, we introduce two main quantities related respectively to the catalytic and gas phase processes:

- the total surface heat release rate:

$$Q_s = -\int_{y_w}^{y_w+l_w} \sum_{k=1}^{n} h_k M_k \hat{\omega}_k \ , \qquad (18)$$

- and the total gas phase heat release rate:

$$Q_g = -\int_0^l \int_0^h \sum_{k=1}^{n} h_k M_k \omega_k \ , \qquad (19)$$

where l is the channel length, h the channel width, y_w the vertical location of the catalytic plate, and l_w its length. Fig. 4 allows a direct identification of the PAR operation regimes thanks to the relative importance of the surface and gas phase heat release rates. Then, according to the inlet hydrogen molar fraction, we define:

- the catalytic regime: no combustion from 0 vol.% to 5.4 vol.% of hydrogen,
- the transition regime: equivalence between catalytic and gas phase processes from 5.4 vol.% to 10 vol.% of hydrogen,
- the gaseous regime: negligible catalytic process from 10 vol.% to 20 vol.% of hydrogen.

The transition regime is characterized by the onset of combustion, so that its frontier with the catalytic regime (i.e. the turning point at 5.4 vol.% H_2) marks a first characterization of the PAR hydrogen ignition limit.

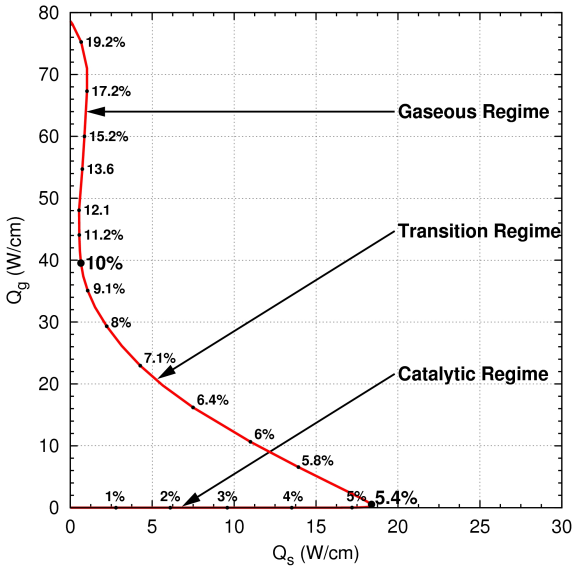

Fig. 4. Regimes for PAR operation

IV.C. Hydrogen ignition criterion

The total gas phase heat release rate has a sudden increase at 5.4 vol.% of hydrogen when the gas phase combustion occurs. On this basis, we define a criterion for the onset of combustion, and so for the PAR hydrogen ignition limit, by the intersection of the tangent to the inflection point of the total gas phase heat release rate curve with the horizontal axis of the inlet hydrogen molar fraction (Fig. 5).

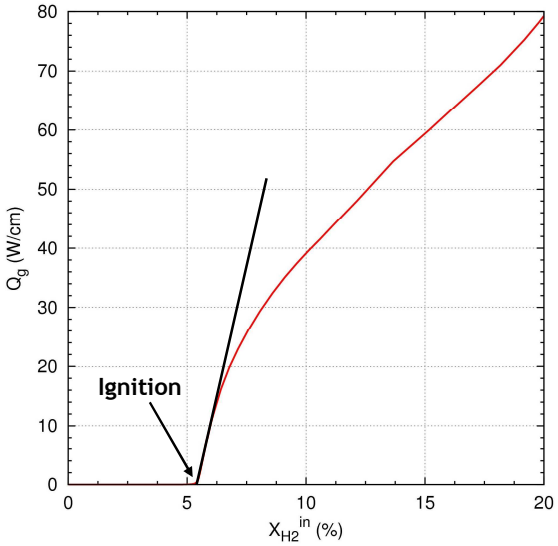

Fig. 5. PAR hydrogen ignition criterion

This method has been applied to identify ignition distances inside catalytic channel reactors (Ref. 15).

Thus, as previously, the upper ignition limit on the segment without steam is evaluated at 5.4 vol.% of hydrogen, what is in perfect agreement with the database from H2PAR and KALI-H2 experiments (Refs. 2,4). The easy implementation of the ignition criterion makes it very useful for large computing campaigns, e. g. the calculation of the whole PAR hydrogen ignition limit presented in the next section.

V. HYDROGEN IGNITION LIMIT INSIDE PAR

After the characterization of the PAR hydrogen ignition without steam, this section describes the methodology to determine the PAR hydrogen ignition limit in the whole ternary diagram H_2–Air–H_2O. The latter aims at representing the possible reactor containment atmospheres in case of a hypothetical severe accident.

V.A. Strategy for the PAR hydrogen ignition limit

The evaluation of the PAR hydrogen ignition limit in the ternary diagram implies a numerical strategy to keep a reasonable CPU time cost. Actually, considering a few hours per solution and a sufficient molar fraction step in the ternary diagram (around 0.1 vol.%), the cost to compute the whole ternary diagram becomes rapidly prohibitive. Then, the strategy to reduce the total CPU time is to cover the diagram only according to segments chosen on the basis of the flammability limit due to Shapiro (Ref. 25). The segments are distributed in 3 zones with specific orientation and direction as illustrated in Fig. 6.

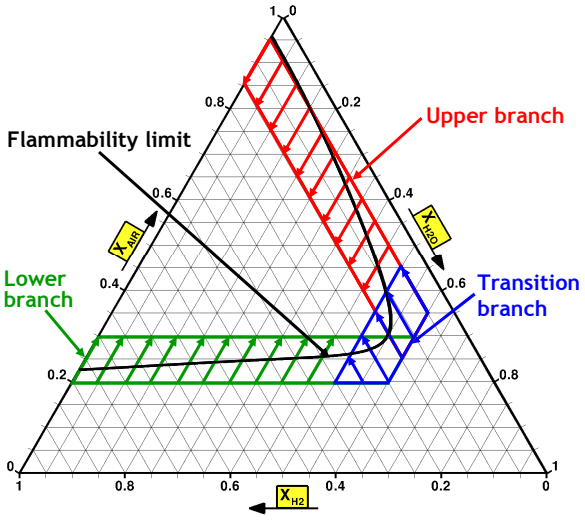

Fig. 6. Strategy for the PAR hydrogen ignition limit

So, we define the upper branch for low hydrogen concentrations (i.e. $X_{H2} < 20\%$), the lower branch for low air concentrations (i.e. $X_{Air} < 30\%$), and the transition branch for high steam concentrations (i.e. $X_{H2O} > 50\%$). The numerical conditions are identical to those of Tab. 3, except the composition of the inlet mixture. This first evaluation of the PAR hydrogen ignition limit has needed more than 500 solutions, spread over more than 30 segments.

V.B. Analysis of the solution branches

V.B.1. Upper branch

The upper branch is characterized by low hydrogen concentrations and a progressive transition from the catalytic regime to the gaseous one (Fig. 7). For each steam concentration, the surface heat release rate increases linearly until it reaches a maximum, and decreases rapidly.

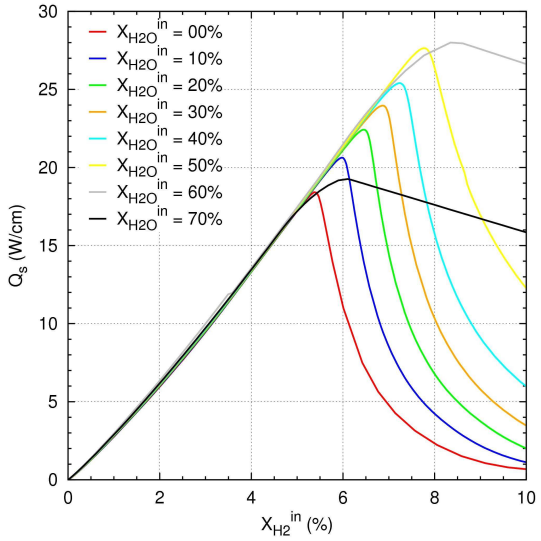

a. On the surface

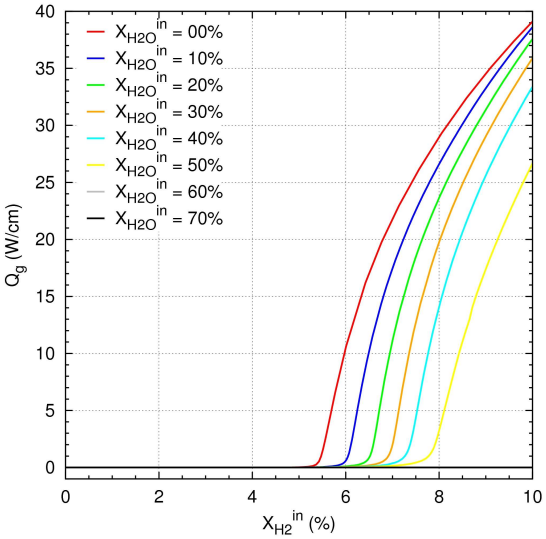

b. In the gas phase

Fig. 7. Heat release rate along the segments of the upper branch

In parallel, the gas phase heat release rate expresses the onset of combustion with a sudden growth systematically below 10 vol.% of hydrogen at inlet. The absence of combustion for 60 vol.% and 70 vol.% of steam leads to a slow decrease of the surface heat release rate beyond its maximum.

It is interesting to notice that before the ignition the surface heat release rate is perfectly independent of the inlet steam concentrations. At the same time, below 5 vol.% of hydrogen, the maximal surface temperature lies on a common linear tendency whatever be the steam inlet concentration (Fig. 8). Moreover, the slope of the temperature curves is not significantly modified when the hydrogen ignition occurs. For high inlet steam concentrations (i.e. without ignition), the temperature rapidly reaches a maximum, before the maximum of the total surface heat release rate.

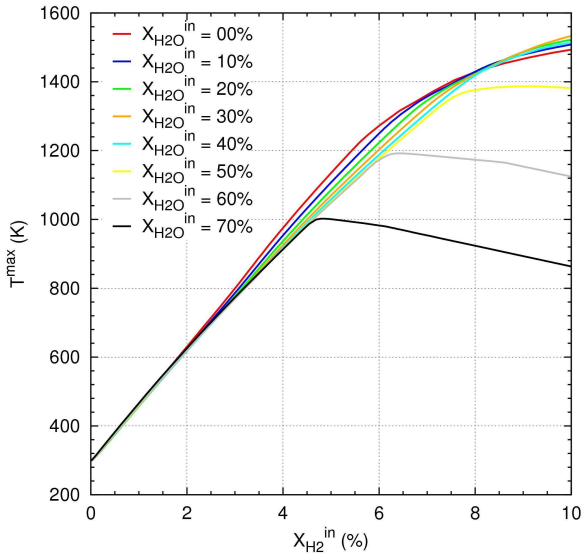

Fig. 8. Maximal surface temperature along the segments of the upper branch

Finally, the similar evolution of the maximum surface temperature and the different inlet hydrogen concentrations at combustion onset show that the surface temperature cannot be sufficient to characterize the hydrogen ignition limit.

V.B.2. Lower and transition branches

At the opposite of the previous upper branch, the lower and transition branches are characterized by a sharp transition from the catalytic regime to the gaseous one (Fig. 9). This sudden onset of combustion can be related to recent experimental observations about the flammability of hydrogen/air mixtures (Ref. 26). Indeed, the study of the hydrogen flammability limit has also revealed two kinds of transition from the slow flame regime (i.e. deflagration) to the accelerated flame regime. For the upper part of the limit the transition was progressive, while for the lower part the transition was abrupt. Nevertheless, the discontinuity observed in the evolution of the heat release rate imposes additional numerical investigations to corroborate this possible analogy between the PAR ignition limit and the classical flammability limit.

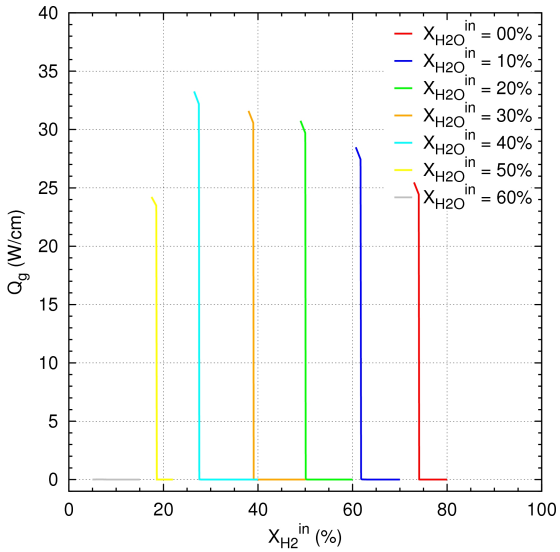

Fig. 9. Heat release rate along the segments of the lower branch

V.C. Experimental validation

The application of the ignition criterion on the different segments of the limit branches allows a first characterization of the PAR hydrogen ignition limit in the ternary diagram. This numerical limit has been validated using the experimental data from Section II. Fig. 10 reveals a satisfying agreement between the experimental and numerical PAR ignition limits.

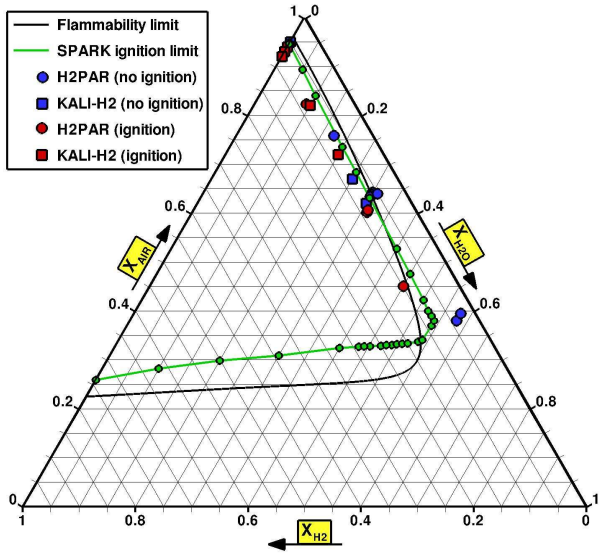

Fig. 10. Experimental and numerical PAR hydrogen ignition limits

It results that the SPARK code now accounts for a relevant numerical tool for extensive studies of hydrogen ignition inside PARs.

The flammability limit for hydrogen/air mixtures in Fig. 10 aims to illustrate the analogy between this classical limit and the PAR hydrogen ignition limit. The latter remains beyond the flammability limit, except near the turning point of the transition branch at high steam concentrations. This observation would mean that such a non-flammable mixture in the containment could ignite through the recombiner. However, the sparse distribution of the experimental points and their relative dispersion appeal additional experimental campaigns to corroborate these first results.

VI. CONCLUSIONS

Numerical simulation of hydrogen ignition by passive auto-catalytic recombiners has been performed with the dedicated numerical tool SPARK developed at IRSN. The detailed analysis about the onset of combustion has pointed out three typical regimes for PAR operations: the catalytic regime, the transition regime, and the gaseous regime. Then, an ignition criterion has been defined by using the total gaseous heat release rate, which is directly related to the production of OH radical during hydrogen combustion. On the basis of this criterion, a specific numerical strategy has allowed a first evaluation of the PAR hydrogen ignition limit in the whole ternary diagram (H_2, Air, H_2O). The calculations have led to a satisfying agreement between the experimental and numerical ignition limits.

This study has also revealed the local intersection of the PAR hydrogen ignition limit with the classical flammability limit (i.e. without recombiner). It results a possible PAR ignition of non-flammable mixtures outside the recombiners. Now, this observation will have to be corroborated by additional campaigns on dedicated PAR facilities. All the more, the experimental data remains sparse, and slightly dispersed. In this sense, the THAI program (Ref. 5) has recently produced an interesting database for PAR hydrogen ignition which tends to confirm and extend the current experimental limit. Moreover, future experiments on the REKO facilities developed at JÜLICH (Ref. 27) should contribute to a deeper analysis of the ignition phenomenon with a detailed validation of PAR operation during combustion, and also to a better definition of the experimental PAR hydrogen ignition limit.

In the future, the PAR ignition limit evaluated in this paper will be refined by considering radiative heat losses and full multi-component transport. Then, the PAR ignition limit at normal conditions could be extended at a wider range of operation pressure and temperature. Finally, the numerical strategy developed for the hydrogen ignition could be applied to carbon monoxide and/or a combination of these flammable gases.

REFERENCES

1. A. Bentaïb et al, “Evaluation of the impact that PARs have on the hydrogen risk in the reactor containment: methodology and application to PSA level 2”, *Proc. TOPSAFE*, Dubrovnik, Croatia, Sept. 30 - Oct. 3, (2008).
2. D. Leteinturier et al, “Essais H2PAR : période mi-98 à fin-2000, Synthèse des essais, Conclusions du programme”, Technical Report, IRSN, DPEA/DIR/02/01, (2002).
3. P. Rongier et al, “Studies of catalytic recombiner performances in H2PAR facility”, *Proc. CSARP*, Bethesda, USA, May 5-8, (1997).
4. O. Braillard, “Test of passive catalytic recombiners (PARs) for combustible gas control in nuclear power plants”, Proc. 2nd International Topical Meeting on Advanced Reactor Safety ARS, Vol. 97, pp. 541-548, (1997).
5. M. Sonnenkalb, G. Poss, “The International Test Programme in the THAI Facility and its Use for Code Validation”, Proc. EUROSAFE, Brussels, Belgium, November 2-3, (2009).
6. N. Meynet and A. Bentaib, “SPARK - Logiciel de calcul pour les recombineurs catalytiques Version 1.0”, IRSN, Technical Report DSR/SAGR/03, (2008).
7. N. Meynet et al, “Detailed Experimental and Numerical Study of Passive Auto-catalytic Recombiners”, *Proc. Second International Meeting of the Safety and Technology of Nuclear Hydrogen Production, Control and Management*, American Nuclear Society, San Diego, USA, June 13-16, (2010).
8. S.B. Dworkin, B.A.V. Bennett, and M.D. Smooke, “A mass-conserving vorticity-velocity formulation with application to non-reacting and reacting flows”, *Journal of Computational Physics*, **215**, pp. 430-447, (2006).
9. A. Ern and M.D. Smooke, “Vorticity-Velocity Formulation for Three-Dimensional Steady Compressible Flows”, *Journal of Computational Physics*, **105**, pp. 58-71, (1993).
10. V. Giovangigli, “Multicomponent Flow Modeling”, Birkhauser Ed., Boston, (1999).
11. A. Ern and V. Giovangigli, “Fast and Accurate Multicomponent Transport Property Evaluation”,

Journal of Computational Physics, **120**, pp. 105-116, (1995).

12. J. Warnatz, R.W. Dibble, and U. Mass, "Combustion, Physical and Chemical Fundamentals, Modeling and Simulation", Springer-Verlag Ed., New York, (1996).
13. O. Deutschmann et al, "Numerical modeling of catalytic ignition", Twenty-Sixth Symposium (International) on Combustion, Edition The Combustion Institute, pp. 1747-1754, (1996).
14. G. Bergeret, "Characterization of metallic catalysts by X-ray and electron microscopy techniques", in Catalysis by metals, Les Editions de Physique Ed., pp 167-180, (1997).
15. C. Appel et al, "An Experimental and Numerical Investigation of Homogeneous Ignition in Catalytically Stabilized Combustion of Hydrogen-Air Mixtures over Platinum", *Combustion and Flame*, **128**, pp. 340-368, (2002).
16. N. Meynet, "Simulation numérique de la combustion d'un propergol solide", Ph.D. Thesis, Paris 6 University, (2005).
17. A. Ern, C.C. Douglas, and M.D. Smooke, "Detailed chemistry modeling of laminar diffusion flames on parallel computers", *The International Journal of Supercomputer Applications*, **9**, n°3, pp. 167-186, (1995).
18. P. Deuflhard, "A Modified Newton Method for the Solution of Ill-Conditioned Systems of Nonlinear Equations with Application To Multiple Shooting", Numerical Mathematics, Springer Verlag Ed., **22**, pp. 289-315, (1974).
19. A. Ern et al, "Towards Polyalgorithmic Linear System Solvers For Nonlinear Elliptic Problems", *SIAM Journal on Scientific Computing*, **15**, n°3, pp. 681–703, (1994).
20. V. Giovangigli and N. Darabiha, "Vector computers and complex chemistry combustion", Mathematical Modeling in Combustion and Related Topics, C. Brauner and C. Schmidt-Laine Ed., Vol. 140, pp. 491-503, (1988).
21. R.J. Kee, F.M. Rupley, and J.A. Miller, "CHEMKIN II: A Fortran Chemical Kinetics Package for the Analysis of Gas Phase Chemical Kinetics", Sandia National Laboratories, Technical Report SAND89-8009B, (1989).
22. R.J. Kee et al, "SURFACE CHEMKIN: A Software Package for the Analysis of Heterogeneous Chemical Kinetics at a Solid-Surface - Gas-Phase Interface", CHEMKIN Collection Release 3.6, Reactor Design Inc., San Diego, (2000).
23. A. Ern and V. Giovangigli, "EGLIB: A general purpose Fortran library for multicomponent transport property evaluation", CERMICS, Technical report n° 96-51, (1996).
24. K. Khose-Höinghaus et al, "Combustion at the focus : laser diagnostics and control", *Proceedings of the Combustion Institute*, The Combustion Institute Ed., Vol. 30, pp. 89-123, (2005).
25. Z.M. Shapiro and T.R. Moffette, Atomic Energy Commission, Technical Report, WAPD-SC-545, USA, Pittsburgh, (1957).
26. H. Cheikhravat et al, "Flammability limits of Hydrogen/Air mixtures", *Proc. Second International Meeting of the Safety and Technology of Nuclear Hydrogen Production, Control and Management*, American Nuclear Society, San Diego, USA, June 13-16, (2010).
27. E.-A. Reinecke et al, "Open issues in the applicability of recombiner experiments and modelling to reactor simulations", Progress in Nuclear Energy, **52**, pp. 136-147, (2010).